

François Faure · Gilles Trolliard · Christian Nicollet
Jean-Marc Montel

A developmental model of olivine morphology as a function of the cooling rate and the degree of undercooling

Received: 31 January 2002 / Accepted: 20 December 2002 / Published online: 26 March 2003
© Springer-Verlag 2003

Abstract We performed dynamic crystallization experiments in the CMAS system at 1 atm to investigate the evolution of the morphology of forsterite crystals as a function of cooling rate and degree of undercooling. In sections parallel to the (010) plane, we observed the evolution of the forsterite morphology from tablets to hopper (skeletal) crystals, and then to swallowtail shapes (dendritic morphology) for increased degree of undercooling. The other shapes described in the literature can be interpreted as particular sections of those three shapes. The onset of dendritic growth is due to a competition between the growth of the faces of the initial hopper crystal and dendrite overgrowths. The forsterite dendrites are formed by a succession of units which look like hopper shapes. This result has been tested by an additional set of experiments.

Introduction

Crystals with rapid growth textures are found in many rock types and settings: pillow lavas (Bryan 1972; Kirkpatrick 1978; Kirkpatrick and Hodges 1978),

xenoliths (Faure et al. 2001a), dykes (Ohnenstetter and Brown 1992), comb-layered rocks (Lofgren and Donaldson 1975), chondrules (Hewins et al. 1981; Lofgren and Russell 1986; Lofgren 1989), tektites (Smit et al. 1992), pseudotachylites (Techmer et al. 1996); komatiites (Donaldson 1982; Arndt 1986; Renner et al. 1994; Barnes 1998). Olivine has been the most widely studied rapidly grown mineral (Drever and Johnston 1957; Donaldson 1976, 1977; Kirkpatrick et al. 1983; Arndt et al. 1984; Arndt and Engelhardt 1987; Jambon et al. 1992). Donaldson (1976) defined ten types of olivine morphologies as a function of the cooling rate and the degree of undercooling. However, he proposed no developmental model between the different shapes. On the other hand, several of these morphologies have been observed coexisting side by side in the same rock where the cooling rate was the same (Natland 1979). Sunagawa (1981, 1987) proposed that crystal morphology depends on the degree of supersaturation (or undercooling) and explained the evolution of crystal habit by changes of growth mechanism. We performed experiments in order to link Sunagawa's model to the morphologies of Donaldson. The two fundamental points of this study are: (1) to propose a three-dimensional pattern of the olivine dendrites, (2) to determine a developmental model of forsterite morphologies mainly as a function of undercooling and for restricted influence of the cooling rate.

Experimental procedures

The starting material was glass prepared from a mixture of reagent grade oxides: 51.34% SiO₂, 14.14% Al₂O₃, 17.39% CaO and 17.11% MgO by weight (Fig. 1). The oxides were mixed in an agate mortar, then melted for 24 h at 1,400 °C (about 50 °C above the liquidus) in air in a platinum crucible, then quenched in water. The resulting glass was then ground in an agate mortar. The powder was formed into pellets (3–4 mm in diameter and 1–2 mm thick) and placed on a platinum wire loop at the end of a ceramic rod situated at the hot spot of a one-atmosphere, vertical tube furnace (Donaldson et al. 1975a). The ceramic rod contains a (PtRh₆/PtRh₃₀) thermocouple located within 1 cm of the pellets. The

F. Faure (✉) · C. Nicollet
Laboratoire "Magmas et Volcans",
Observatoire de Physique du Globe de Clermont-Ferrand,
UMR 6524 CNRS, Université Blaise Pascal, 5 rue Kessler,
63038 Clermont-Ferrand Cedex, France
E-mail: f.faure@opgc.univ-bpclermont.fr
Tel.: +33-473-346721
Fax: +33-473-346744

G. Trolliard
Science des Procédés Céramiques et de Traitements de Surface,
UMR 6638 CNRS, 123 avenue Albert Thomas,
87060 Limoges Cedex, France

J.-M. Montel
Laboratoire des Mécanismes de Transfert en
Géologie-Minéralogie, UMR 5563 CNRS,
39 allées Jules Guesde, 31000 Toulouse, France

Editorial responsibility: T.L. Grove

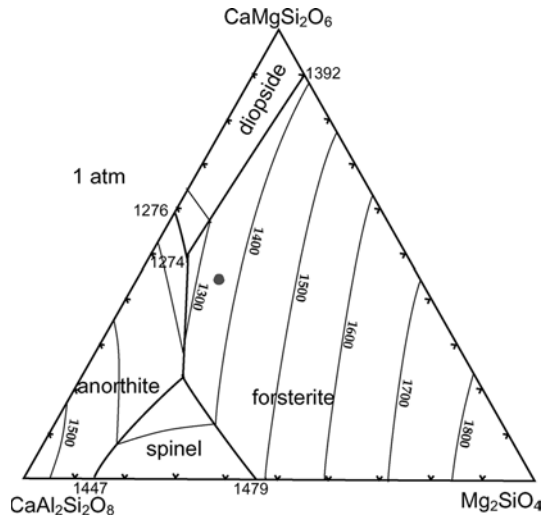


Fig. 1 Projection from SiO_2 component of composition of starting materials (circle) plotted on the liquidus diagram of the system forsterite–diopside–anorthite (after Presnall et al. 1978)

thermocouple was calibrated against the melting points of gold ($1,064^\circ\text{C}$) and palladium ($1,552^\circ\text{C}$). The charges were first melted for 1 h above the liquidus ($22^\circ\text{C} < +\Delta T < 124^\circ\text{C}$), $+\Delta T$: the degree of superheating corresponding to the difference between the annealing temperature and the liquidus temperature. The charges were then cooled at a constant rate varying from 1 to $1,890^\circ\text{C}/\text{h}$ (dynamic crystallization experiment). At the end of the experiments, the samples were quenched by dropping them into water.

In this study, we used the “nominal undercooling” ($-\Delta T$) defined by Kirkpatrick et al. (1981) as liquidus temperature ($T_{\text{liquidus}} = 1,342^\circ\text{C}$ for this composition) minus quench temperature. This nominal undercooling is different from the actual degree of undercooling which is the difference between the actual temperature of a liquid or a liquid-crystal system and the liquidus at some point in time (Lofgren, 1975). In experiments, the “actual degree” of undercooling is generally measured as temperature difference between the liquidus temperature and a temperature plateau at which the sample is maintained for a finite time. However, even with this experimental method, the actual degree of undercooling is not known accurately. This is because during crystallization the liquid composition changes and therefore its liquidus temperature also changes. As a result, the accurate determination of the actual degree of undercooling is complex. In a previous study devoted (1) to the influence of the cooling rate on the heterogeneous nucleation rate, and (2) to chemical investigation of the crystal-liquid interface, we showed that the nominal undercooling is a good approximation of the degree of undercooling when the cooling rate is rapid (Faure 2001). In fact, in this condition, the growth is controlled by diffusion and the chemical composition of the liquid (now glass) is affected by crystal growth only in a narrow zone ($< 100\ \mu\text{m}$) around it. Therefore, liquidus temperature is not changed away from the crystal. For this reason, we have adopted the thermal convention defined by Kirkpatrick et al. (1981).

After experiments, charges were mounted in epoxy and prepared as doubly polished thin sections. The thin sections were studied by optical and scanning electron microscope (SEM). SEM work was carried out on a Cambridge-Leica Stereoscan 360 at Université Blaise Pascal, equipped with an X-ray analyser operating in energy dispersive mode. We used mainly the backscattered electron mode on polished thin sections, with 20-kV accelerating voltage, 2-nA probe current, 17-mm working distance.

Heterogeneous nucleation on platinum wire is a common feature observed in the charge obtained by this experimental method (Berkebile and Dowty 1982; Lofgren 1983; Lofgren and Russell 1986). In order to reduce or eliminate the delay of nucleation

(Walker et al. 1976; Donaldson et al. 1975b) and then obtain all steps of olivine growth, we decided to take advantage of this phenomenon, and platinum impurities were added to the starting glass.

Description of morphologies

Five different morphologies have been distinguished: polyhedral, tabular, skeletal, dendritic and feather shape. Results of dynamic crystallization experiments are presented in Table 1. The olivine crystallises with the Pbnm space group and the unit cell $a = 4.75\ \text{\AA}$, $b = 10.19\ \text{\AA}$ and $c = 5.98\ \text{\AA}$.

Polyhedral crystal

Polyhedral shaped crystals always display well-defined faces (Fig. 2). According to Deer et al. (1962), these faces are commonly: $\{010\}$, $\{021\}$, $\{110\}$, $\{120\}$ and $\{101\}$. These crystals generally contain spherical or elongated glass inclusions.

Tabular morphology

Crystals display a tabular habit (Fig. 3). The crystal growth is preferentially developed in the $[100]$ and $[001]$ directions and less in the $[010]$ direction. The rectangular shape is thus observed when the crystal is orientated under $[010]$ zone axis. For sections normal to (010) , the crystal has a needle-like shape. The tabular shape is less common than other morphologies and it is always associated with polyhedral or hopper crystals.

Skeletal forsterite: hopper morphology

At first glance, two morphologies seem to be evident in Fig. 4A. Some crystals have an hexagonal shape while others display an hourglass morphology. In fact, they are the same, but viewed along different zone axes. The hourglass shape corresponds to observations roughly orientated under the $[010]$ direction, while hexagonal sections (Fig. 4A, B) represent observations along $[100]$. Figure 4A shows hopper crystals are prismatic, elongated along the $[100]$ direction. Figure 4B shows that the external faces of the prism are mainly (010) and $\{021\}$. A peculiarity of hopper crystals is that the top of the prism is not limited by well-defined (100) faces, but terminates in large cavities filled with glass (Fig. 4A). This hollow is typical of hopper crystals. The morphology of the cavity corresponds to a concentric stair-like microstructure (Fig. 4B).

An interpretative sketch of the hopper crystal morphology is presented Fig. 4C. When observed under the $[010]$ direction, the cavity gives rise to the specific hourglass morphology, which is better seen under crossed-polars (Fig. 4D, E). These figures show that the

Table 1 Results of dynamic crystallisation experiments. $+\Delta T = T_{\text{initial}} - T_{\text{liquidus}}$, $-\Delta T = T_{\text{liquidus}} - T_{\text{quench}}$, morphologies

Run no.	$+\Delta T =$ $T_{\text{starting}} - T_{\text{liquidus}}$ (°C)	dT/dt (°C/h)	T_{quench} (°C)	$-\Delta T =$ $T_{\text{liquidus}} - T_{\text{quench}}$ (°C)	Morphologies of forsterite ^a	Other minerals and comments
F2/337	34	1	1,298	44	P	Pt capsule
F2/573	40	2	1,318	24		*
F2/576	38	2	1,300	42		*
F2/422	52	2	1,280	62		*
F2/518	43	2	1,272	70		*
F2/577	38	2	1,268	74		*
F2/578	38	2	1,262	80		*
F2/545	22	2	1,226	116	P	D pyroxene
F2/325	32	9.6	1,294	48	P + T	
F2/272	29	45.5	1,294	48	H	
F2/520	42	47	1,308	34	P + H	
F2/320	32	47	1,298	44	P + T	
F2/318	32	47	1,296	46	H	
F2/319	32	47	1,293	49	H	
F2/488	57	47	1,156	186	H	D pyroxene
F2/286	30	97.5	1,294	48	T + H	
F2/293	124	97.5	1,286	56	H	
F2/352	43	188	1,308	34	H	
F2/356	43	188	1,298	44	H	
F2/353	44	188	1,292	50	H	
F2/355	43	188	1,286	56	H	
F2/354	44	188	1,276	66	H	
F2/357	43	188	1,262	80	H + "b"	
F2/308	32	225	1,322	20	H	Only one crystal
F2/309	33	225	1,302	40	H	
F2/344	34	225	1,298	44	H	
F2/312	33	225	1,293	49	H	
F2/310	34	225	1,290	52	T + H	
F2/343	34	225	1,287	55	H	
F2/288	30	225	1,262	80	H	
F2/326	32	225	1,261	81	H + "b"	
F2/338	33	225	1,166	176	D	Pt capsule
F2/341	33	225	1,106	236	D	
F2/359	42	361	1,290	52	H	
F2/360	42	361	1,282	60	H	
F2/361	42	361	1,276	66	b + H	
F2/362	42	361	1,271	71	b	
F2/369	42	361	1,266	76	b	
F2/287	31	422	1,274	68	H	
F2/418	42	447	1,196	146	D	
F2/365	42	525	1,276	66	H + "b"	
F2/364	42	525	1,270	72	b	
F2/366	42	525	1,261	81	"b"	
F2/432	44	670	1,234	108	D	
F2/429	46	670	1,196	146	D	
F2/367	42	692	1,276	66	H	
F2/368	42	692	1,266	76	b	
F2/371	42	692	1,250	92	b	
F2/292	30	758	1,288	54	H	
F2/373	42	837	1,272	70	b	
F2/374	42	837	1,258	84	b	
F2/375	42	837	1,242	100	b + D	
F2/431	44	886	1,194	148	D	
F2/400	43	991	1,291	51	H	
F2/399	43	991	1,282	60	"H"	
F2/396	43	991	1,272	70	H	
F2/398	43	991	1,264	78	b	
F2/397	43	991	1,254	88	b	
F2/401	42	991	1,245	97	D	
F2/402	44	991	1,238	104	D	
F2/377	42	1,155	1,290	52	H	
F2/376	42	1,155	1,250	92	b	
F2/380	42	1,155	1,226	116	D	
F2/295	30	1,246	1,282	60	H	
F2/575	48	1,552	1,282	60	H + b	

Table 1 (Contd.)

Run no.	$+\Delta T = T_{\text{starting}} - T_{\text{liquidus}}$ (°C)	dT/dt (°C/h)	T_{quench} (°C)	$-\Delta T = T_{\text{liquidus}} - T_{\text{quench}}$ (°C)	Morphologies of forsterite ^a	Other minerals and comments
F2/541	50	1,552	1,242	100	D	
F2/297	30	1,890	1,284	58	H	
F2/510	44	1,890	1,274	68	b	
F2/509	44	1,890	1,238	104	D	
F2/329	33	1,890	1,220	122	D	
F2/527	42	1,890	1,208	134	D	
F2/296	30	1,890	1,186	156	D	
F2/519	41	1,890	1,177	165	D	
F2/525	41	1,890	1,152	190	D	
F2/507	46	1,890	1,126	216	D	
F2/515	45	1,890	1,126	216	D	
F2/506	46	1,890	1,100	242	D	
F2/332	33	1,890	1,084	258	D	
F2/458	36	1,890	1,076	266	D	
F2/408	42	1,890	1,063	279	D	
F2/490	38	1,890	1,019	323	D	
F2/487	36	1,890	1,004	338	D	
F2/491	36	1,890	1,001	341	D	
F2/481	36	1,890	1,000	342	D	
F2/333	33	1,890	986	356	D	

^a *P* Polyhedral, *T* tablet, *H* hopper, *b* baby swallowtail, *D* dendrite (swallowtail, rods), * beginning of the shape, * charges were cooled at 1,725 °C/h before quenching

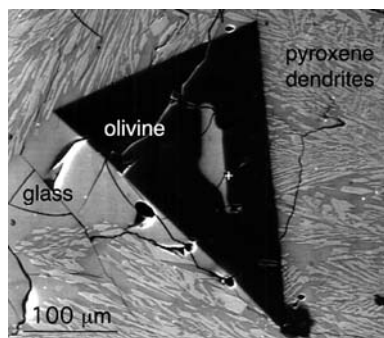


Fig. 2 SEM image of a polyhedral forsterite. Note the large rounded glass inclusion located at the centre of the crystal. The charge is crowded by dendritic pyroxenes (cooling rate: 2 °C/h; $-\Delta T = 116$ °C)

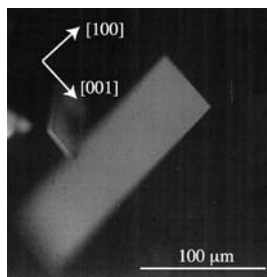


Fig. 3 Photomicrograph of tabular crystal observed along [010] zone axis (cooling rate: 97.5 °C/h; $-\Delta T = 48$ °C)

shape of the cavity depends on the size of the hopper crystals. In smaller crystallites (Fig. 4D), the cavities are V-shaped and the interface between the crystal and the glassy pockets does not present a step-like morphology,

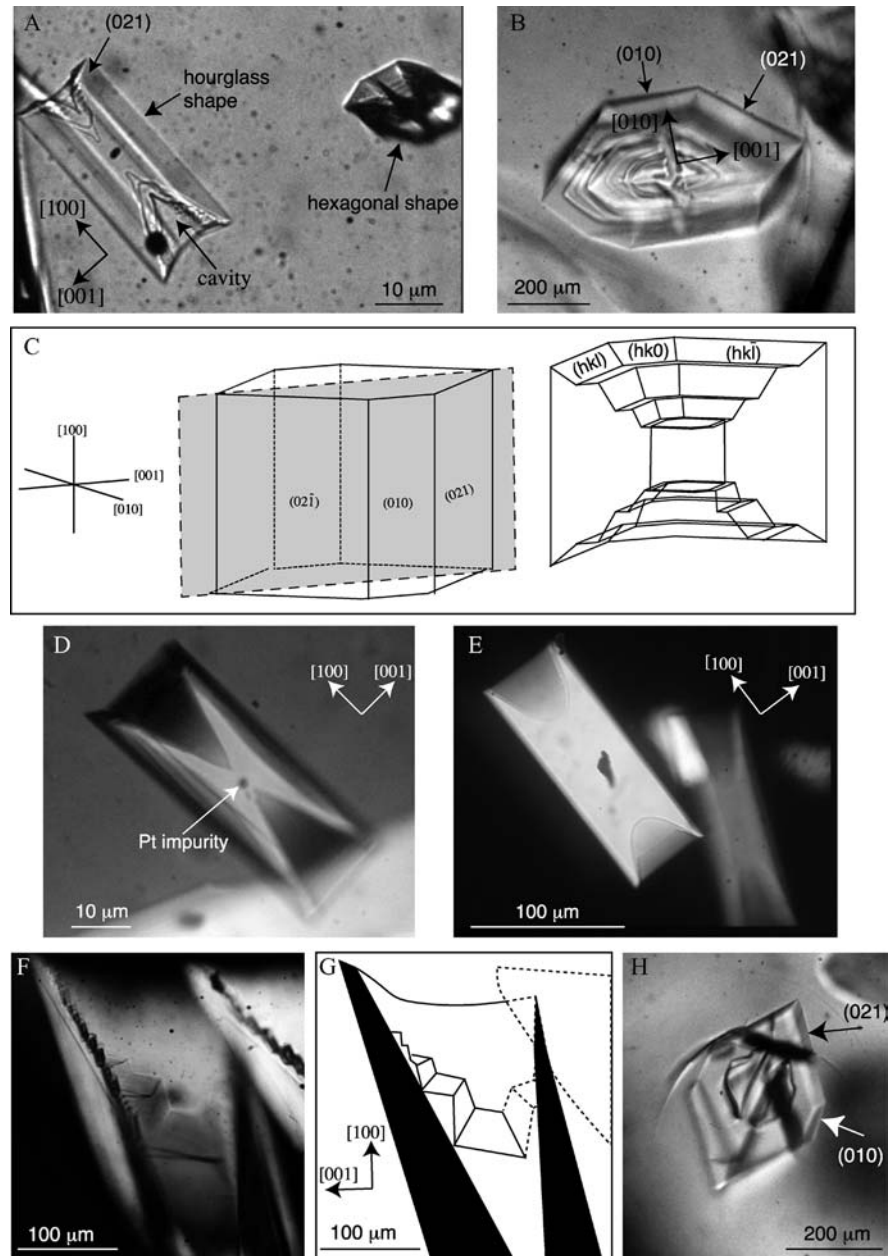
at least at the scale of optical microscopy. In larger crystals, however, the cavity has a U-shape and the glass-crystal interface always exhibits step morphology (Fig. 4B, F, G). With regard to the [100] direction, the step morphology is built up of oblique faces (of the {hk0} and {hkl} types) which alternate along [100] with (100) faces (Fig. 4G). Such macrosteps, whose sizes range from a few microns to about 10 μm, have been described and interpreted as a growth texture by Chernov and Nishinaga (1987).

The development of the stair-like morphology is strongly influenced by the thermal treatment. If the cooling rate of the sample is high, vicinal faces are formed and the step morphology is poorly developed. On the other hand, when the sample is briefly maintained isothermally, i.e. few minutes of annealing treatment before being quenched, the step morphology is apparent at the optical scale (Fig. 4B). These results suggest that the steps correspond to macroscopic growth ledges. This growth-ledge mechanism takes place to fill up the cavity situated at the top of the hopper crystal. This inference is supported by further experiments in which samples were annealed for several hours before quench. In these, hopper crystals are seldom seen and hopper cavities are always filled up by the growth of olivine (Fig. 4H).

Dendritic forsterite: swallowtail and rod morphologies

The dendrites present a (010) discoid shape. Swallowtail shape (Figs. 5, 6) corresponds to a section parallel to (010) plane of dendritic forsterite and represents a plane view of the dendrite while rod morphology (Fig. 8) corresponds to a cross section of the dendrite.

Fig. 4 Photomicrographs of hopper morphology. **A** Hourglass and hexagonal shapes together (cooling rate: 225 °C/h; $-\Delta T = 80$ °C). **B** Hexagonal shape observed in section parallel to (100) plane showing the stair-like texture (cooling rate: 47 °C/h; $-\Delta T = 48$ °C, crystal stayed isothermally 3 min at quench temperature). **C** Interpretative sketch of hopper crystal morphology. **D** Small hourglass-shaped hopper crystal observed in section parallel to (010) plane. Under crossed-polarised light the cavities are revealed by a strong contrast due to the presence of the glass. The end of the hourglass cavity has a V-shape (cooling rate: 692 °C/h; $-\Delta T = 76$ °C). **E** Large hopper crystal showing a more complex cavity. The end is more or less flat (U-shape) due to the presence of a tabular olivine (cooling rate: 422 °C/h; $-\Delta T = 68$ °C). **F** The internal part of the hopper cavity which shows macrosteps (cooling rate: 188 °C/h; $-\Delta T = 56$ °C). **G** Interpretative sketch of **F**. **H** The cavity of the hexagonal shape starts to fill up when the crystal stays 30 min at quench temperature (cooling rate: 225 °C/h; $-\Delta T = 49$ °C)



Swallowtail crystals have a straight extinction and are grey in crossed polars. Indexation of crystallographic faces (Fig. 5) has been confirmed by electron diffraction experiments (Faure and Troliard 1999). Two shapes are distinguished, depending on the degree of development of the dendrite but not the size of crystals: baby swallowtail shape at the beginning of the dendritic growth and swallowtail morphology when the dendrites are well developed. These shapes are seen as hopper crystals which have dendrite overgrowths.

Baby swallowtail shape

This shape displays an hourglass crystal (hopper crystal) in the centre, similar to those described above, and

overgrowths are observed inside the cavity of this hopper crystal (Fig. 5A, B). Their thickness in the [010] direction is few microns and these overgrowths are actually elongated in the [100] direction.

Figure 5C, D displays a section with a large tilt to [100]. One overgrowth extends from the cavity of a hopper crystal and is delimited by external {021} and (010) crystalline faces. Slight focus variations performed with the optical microscope reveal that these overgrowths are also hollow shaped, with a central cavity filled by glass. Figure 5A, B show that these overgrowths look like half hourglass crystals when observed under [010] zone axis direction.

These features indicate that overgrowths in the hopper crystal cavities are built up in a way similar to the hopper crystals themselves and consequently have the

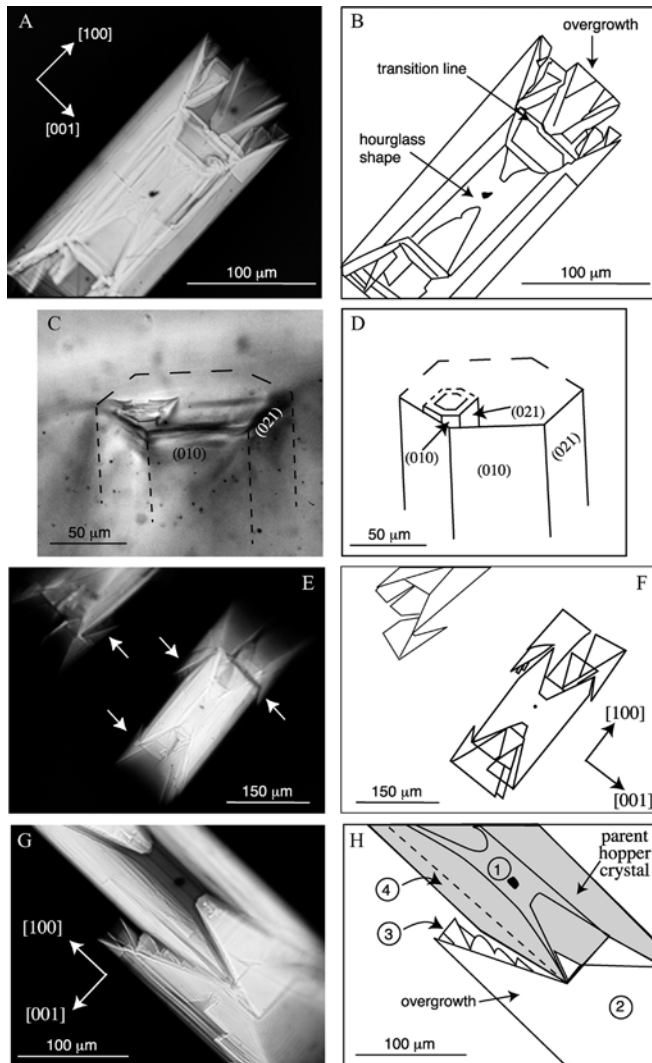


Fig. 5 Photomicrographs and interpretative sketches of baby swallowtail morphology. **A** Baby swallowtail olivine displaying an hourglass shape in the centre. Overgrowths develop inside the cavity of the hopper crystal but never at the end of the hole (cooling rate: $692\text{ }^{\circ}\text{C/h}$; $-\Delta T = 76\text{ }^{\circ}\text{C}$). **B** Interpretative sketch of **A**. **C** Baby swallowtail morphology observed in section tilted with regard to $[100]$ zone axis. Overgrowth displays the same morphology as hopper crystal: (010) and (021) faces and cavity filled by glass (cooling rate: $361\text{ }^{\circ}\text{C/h}$; $-\Delta T = 71\text{ }^{\circ}\text{C}$). **D** Interpretative sketch of **(C)**. **E** Overgrowths forming tablets which develop around the hopper crystal (cooling rate: $991\text{ }^{\circ}\text{C/h}$; $-\Delta T = 88\text{ }^{\circ}\text{C}$). **F** Interpretative sketch of **E**. **G** Different growth steps observed on a baby swallowtail crystal (cooling rate: $525\text{ }^{\circ}\text{C/h}$; $-\Delta T = 72\text{ }^{\circ}\text{C}$). **H** Interpretative sketch of **G**. 1 represents the initial hourglass shape (hopper crystal). 2 A large hourglass develops inside the hopper crystal and protrudes outside of the cavity. This large overgrowth develops around the hopper crystal but is never in contact with it. 3 Second generation of overgrowths on the first large one. The second generation prevents growth of the hopper crystal in this zone. 4 The zone of parent hopper crystal which is not in competition with overgrowths can grow

same morphology. They can be considered as secondary sets of hopper crystals. It is evident that overgrowths are only located in the upper part of the cavity of the parent hopper crystal. These overgrowths never start to grow

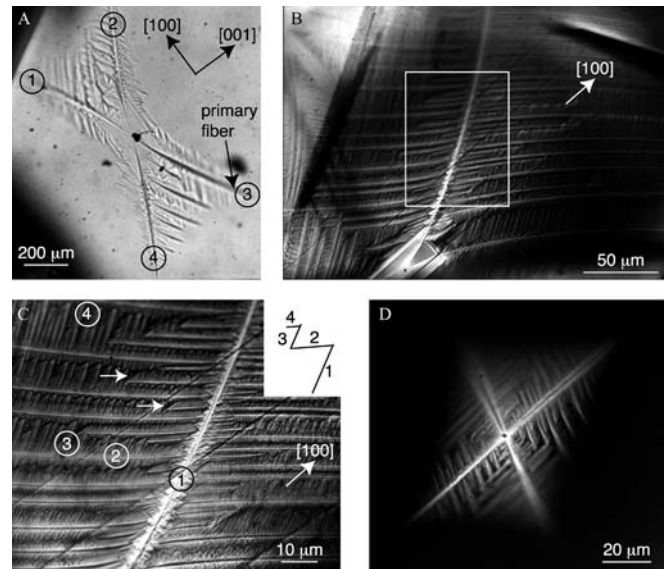


Fig. 6 Photomicrographs of swallowtail olivines observed in section parallel to (010) plane. **A** Swallowtail crystal displaying dendritic fibres which develop from corners of the hopper crystal (cooling rate: $1,890\text{ }^{\circ}\text{C/h}$; $-\Delta T = 122\text{ }^{\circ}\text{C}$). **B** When undercooling increases, the swallowtail crystal develops along $[100]$ and $[001]$ directions and constitutes a complex dendritic feature (cooling rate: $1,890\text{ }^{\circ}\text{C/h}$; $-\Delta T = 216\text{ }^{\circ}\text{C}$). **C** Enlargement of the squared area in **B** showing four generations of dendritic fibres and their relationships. The four directions of fibres and their relative chronology are identified on the upper right side of the photo. *Arrows* show the relationships between fibres of the three last generations. **D** Small swallowtail olivine which seems to have no hourglass shape in the centre and grew directly on a platinum impurity (cooling rate: $1,890\text{ }^{\circ}\text{C/h}$; $-\Delta T = 134\text{ }^{\circ}\text{C}$)

from the bottom of the hopper cavity. In fact, each cavity of the parent hopper crystals presents a boundary (named “transition line” on Fig. 5B) above which the overgrowths can grow. However, near this transition line, the size of the observed overgrowths is generally very small. The size of the latter gradually increases as their position moves toward the upper part of the cavity. Some are sufficiently developed to surround the parent hopper crystal (Fig. 5E, F, arrows). Figure 5G, H shows a secondary set of hopper crystals (overgrowth: 2) that are more developed than the parent hopper crystal which is easily identified by its central platinum inclusion. Note that the overgrowth presents a cavity containing a secondary set of overgrowths (see 3 in Fig. 5H). This secondary set corresponds to a third generation of hopper crystals. The development of the (001) external face of the parent hopper crystal has been impeded by the growth of the secondary set of overgrowths in Fig. 5G, H. Baby swallowtail morphology is thus the initial degree of the dendritic growth.

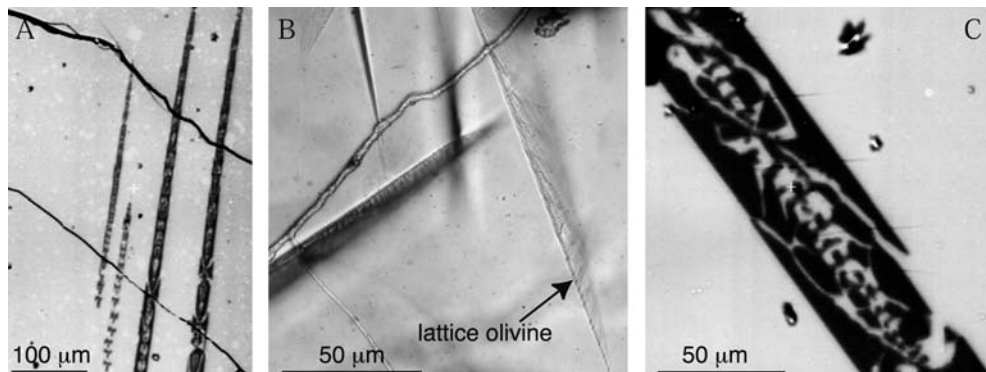
Swallowtail morphology s.s.

Swallowtail morphology can be seen as an hourglass crystal on which dendrites are developed (Fig. 6A). Swallowtail crystals thus differ from baby swallowtails,

by the occurrence of abundant dendritic growth. The dendrites seem to grow on the corners of the prism of the hopper crystal. Dendritic fibres are slightly arching but seem to grow along the [101] and [-101] direction, as previously observed by Donaldson (1976). The relationship between the hopper crystal and the dendrites is seen best between crossed polars (Fig. 6B). The overall dendritic microstructure extinguishes homogeneously. Even the hopper crystal and dendrites extinguish simultaneously, demonstrating their optical and therefore crystallographic continuity.

In more detail, the dendrites are composed of several sets of fibres corresponding to several generations of crystallites. The arrangement of fibres shows generally the same pattern. First, the four principal and primary fibres form the frame of the dendritic domain. The second generation of fibres (labelled 2 in Fig. 6C) develops on the primary ones. The growth of the secondary fibres is not uniform. For example, if we consider Fig. 6A, the set of secondary fibres is more developed on the primary fibres labelled 1 and 4 than on those labelled 2 and 3. This is a general feature and swallowtail microstructures always present two primary fibres on which the set of secondary fibres are better developed and they are always situated on opposite sides of the dendrite, with regard to the (001) plane of the hopper crystal. Figure 6C shows the different generations of fibres developed around hopper crystals. In addition to the sets of primary and secondary fibres, there are third and fourth generation. The directions of these different sets of fibres are reported on the upper right side of Fig. 6C and only two crystallographic directions of growth are found, [101] and [-101]. Some of the fibres of second generation are very short compared to others, in particular when the third generation fibres impede their growth (Fig. 6C, see arrows). This observation suggests there was competitive growth of the fibres of the different generations.

Fig. 8 SEM and optical images of the rods. **A** SEM image of four parallel rods named chain olivine by Donaldson (1976). They are constituted by units apparently more or less connected (cooling rate: 225 °C/h, $-\Delta T = 176$ °C). **B** Photomicrograph of lattice olivine (cooling rate: 1,890 °C/h, $-\Delta T = 258$ °C). **C** SEM image of branching olivine. Note the microfractures which corresponds to [100] direction of olivine and extends into the glass (cooling rate: 225 °C/h, $-\Delta T = 176$ °C)



In agreement with Kirkpatrick et al. (1981), we can see no critical size of the hopper crystal for the onset of dendritic growth. In the same sample, very small swallowtails (1–2 μm for the smallest) are observed near larger ones. Optical microscopy observations suggest that larger dendritic units lack hourglass shape in the centre and grow directly on a platinum impurity (Fig. 6D). However, transmission electron microscopy (TEM) studies confirm that hourglass shape is present at all scales (Faure et al., submitted).

Swallowtail crystal observed directly on the surface of the charge (before being mounted in epoxy) show a pyramidal shape (Fig. 7). The hopper crystal first develops from impurities located on the charge (Fig. 7) and the crystal grows into the charge. This configuration shows that overgrowths are piled up like a pyramid.

Swallowtails may show twin microstructures. Additionally, a few half swallowtail crystals may grow from the same impurity to form a bunch.

As previously mentioned, the rod shape (Fig. 8) corresponds to a cross section of the discoid shaped dendrite. This result is supported by an exhaustive study by TEM (Faure et al. 2001b). The rods correspond to sections performed parallel to (h0l) plane (with h or l possibly equal to zero) of the crystals. When the k index is other than zero, the transverse sections correspond to either lattice olivine (Fig. 8B) or branching olivine (Fig. 8C) in the nomenclature adopted by Donaldson (1976). The dendritic crystals are composed either of a single rod or of small groups of three or four parallel rods (Fig. 8A). It is important to note that when several parallel rods are observed within a thin section, they exhibit a common extinction, attesting that they belong

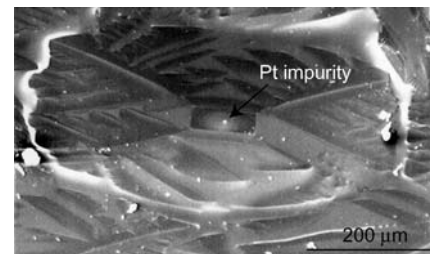


Fig. 7 SEM images of swallowtail crystal observed on the surface of the charge (cooling rate: 1,890 °C/h, cooling beyond the glass transition)

to the same structural entity, i.e. to the same dendrite. These elongated crystals correspond to chain olivine of Donaldson (1976) and in optical microscopy they display a straight extinction when observed in cross-polarised light. Inside the rods, there is a complex microstructure composed of units which have a “flattened Maltese cross” or “ornamental lantern form” (Bryan 1972), termed H-shape by Donaldson (1976). The morphology of these subunits is, however, always very similar to those observed on hopper crystal under reflected light. These units commonly seem to have no inter-connection (Fig. 8A), but their optical continuity proves that they must be in the third dimension.

Feather olivine

Charges which stayed more than 5–6 h isothermally at 800–900 °C display very fine fibres, which developed on the dendritic fibres of the swallowtail crystals (Fig. 9A) as well as on the rods (Fig. 9A, B). However, this fine texture is always observed at the extremity of rods, which corresponds to the periphery of the swallowtail crystals, i.e. the periphery of the discoid shape of the dendrite. When observed in crossed polars, the tiny crystallites and the dendrites extinguish simultaneously. These small olivine crystals are thus perfectly orientated on the swallowtail crystal. As observed by Arndt et al. (1984), these fine fibres are slightly browner than the swallowtail crystals (Fig. 9A). This type of texture could, at first glance, be interpreted as a form of olivine spherulite (Keith and Padden 1963; Lofgren 1971). However, the tiny crystals which compose spherulites are slightly disorientated one to another, which is not the case in the studied system. This is the reason why we prefer to call this peculiar microstructure feather olivine (Fig. 9C), as previously named by Donaldson (1976). It is always associated with dendritic pyroxene in the

sample. Olivine spherulites (Radiate and feather olivines) seem to be due to devitrification rather than dynamic crystallization in our experiments because they always take place near the glass transition.

Summary of the morphologies

Among the ten basic forms proposed by Donaldson (1976), only four of them are retained to illustrate the growth conditions:

- the polyhedral shape,
- the tabular form,
- the hopper morphology,
- the dendrites (baby swallowtail, swallowtail shapes and rods).

Indeed, as previously established, the rods, the lattice olivine, the chain olivine and the branching olivine represent different cross sections of the same kind of crystals: the dendrites (swallowtail morphology).

Thermal parameters: cooling rate versus undercooling

The effects of the cooling rate and the degree of undercooling have already been emphasised by numerous authors (e.g. Donaldson et al 1975b; Coish and Taylor 1979; Lofgren, 1980, 1996). To appreciate the respective influence of the cooling rate and the degree of undercooling on the morphology of olivine crystals, the different habits of olivine crystals present in the charges are shown in a “cooling rate versus undercooling” diagram (Fig. 10).

In this diagram, hopper crystals and baby swallowtail crystals are distinguished as two different groups although baby swallowtail morphology corresponds to an

Fig. 9 Optical and SEM images of feather olivine (cooling rate: 89 °C/h, $-\Delta T = 46$ °C, then the charge is cooled rapidly and stays several hours at 900 °C). **A** Photomicrograph showing fine fibres which develop on swallowtail or rod olivine. **B** Enlargement of the squared area in **A**. Fine fibres have the same orientation as the rod which is used as support. **C** SEM image showing dendritic pyroxene associated with feather olivine

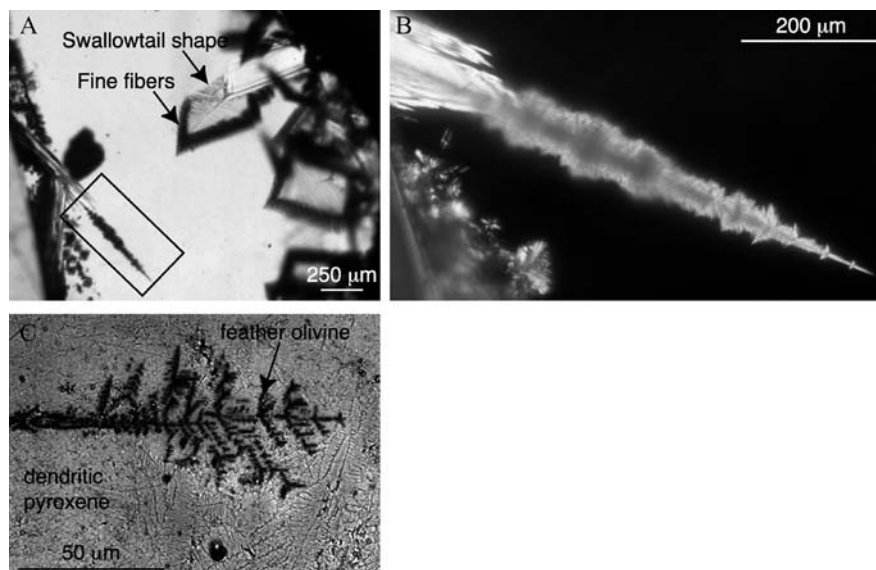
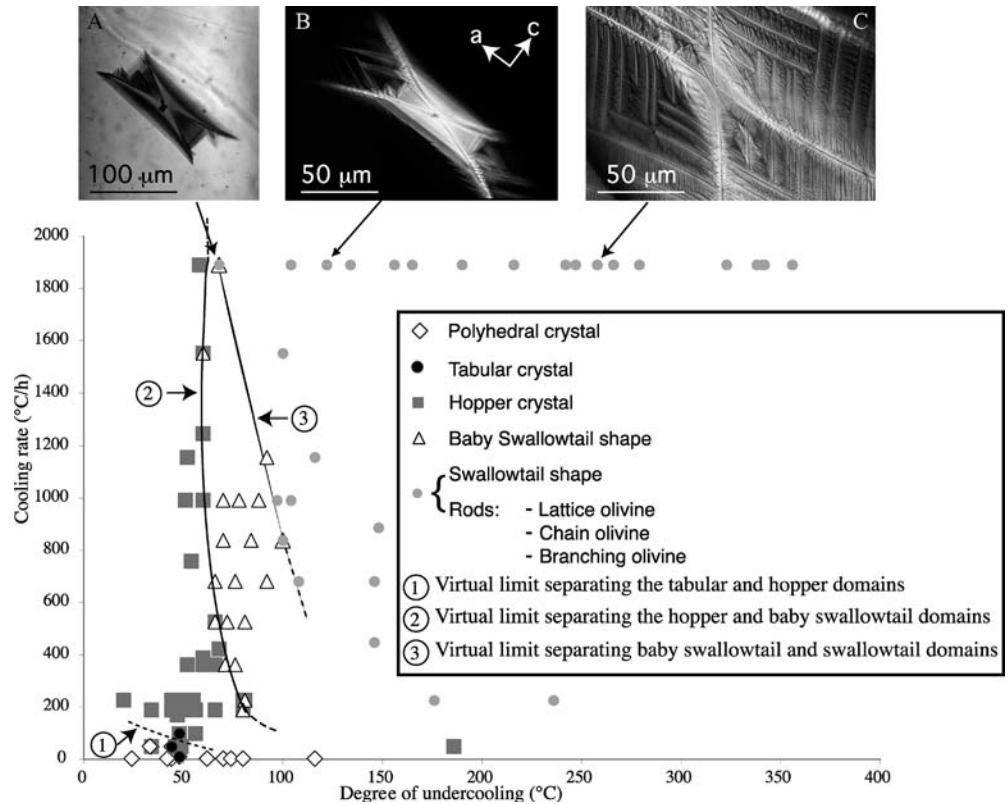


Fig. 10 Morphology variations of olivine as a function of the cooling rate and undercooling. **A, B, C** Evolution of the morphology in section parallel to (010) for a cooling rate of 1,890 °C/h. Swallowtails and rod shapes have been plotted together, using the same symbol because they occur in the same samples. **A** Baby swallowtail shape ($-\Delta T = 68$ °C). **B** Swallowtail shape ($-\Delta T = 122$ °C). **C** For large value of undercooling ($-\Delta T = 258$ °C), the length of the dendritic fibres increases significantly



intermediate stage of evolution between the hopper crystals and the dendritic olivine (see inserts A–C in Fig. 10).

In Fig. 10, the existence of tabular crystals is also reported. Very few experiments created this crystalline shape suggesting that the stability field of this habit is very restricted in this diagram. This morphology is, however, important as these crystals represent the prime evolution towards rapid growth textures (see below). The diagram shows a number of important features.

1. Whatever the degree of undercooling (up to 116 °C), the low cooling rate experiments (2 °C/h) always produce only polyhedral crystals.
2. When the cooling rate increases to 47 °C/h, the presence of polyhedral crystals vanishes progressively and the majority of the crystals are tabular or hopper. The virtual boundary separating these two crystalline habits (polyhedral and tabular) can be considered as the limit between the “steady state” growth shape (polyhedral morphology) and the beginning of the textures of rapid growth (tabular crystals). This limit is indicated by dashed line owing to the lack of data points. Beyond this boundary, the evolution of the morphology of olivine crystals only depends on the degree of undercooling and not on the cooling rate (Fig. 10). The cooling rate changes only the size of the crystals and the transition temperature between the different crystalline forms.
3. When undercooling ranges from 60–90 °C, hopper crystals develop overgrowths depending on the

cooling rate. The resultant morphology is a baby swallowtail shape. Sometimes, in the same charge, hopper crystal and baby swallowtail shape are present together permitting an accurate estimate of the temperature of undercooling transition between the two morphologies. The transition temperature decreases when the cooling rate increases. Other shapes are always present with baby swallowtail crystal. These shapes correspond to small rods (small dendrites).

4. For larger undercooling ($-\Delta T > 70\text{--}90$ °C) as a function of the cooling rate, only swallowtail crystals (dendrites) are present.

Discussion of rapid growth morphologies

To correlate morphological observations between samples, they must be done in the same crystallographic section, and only a section parallel to (010) plane allows observation of crystal as a whole. In this orientation, the evolution pattern is: tablet⇒hourglass⇒baby swallowtail⇒swallowtail.

Evolution tablet⇒hopper crystal (hourglass shape)

The previous section has shown that in experiments conducted at the same cooling rate display different

crystal morphologies as a function of the degree of undercooling. For small undercooling, tablet morphology is observed and when samples are submitted to higher degrees of undercooling, hopper crystals appear. In detail, all these hopper crystals are not identical in the same charge regarding the slope of their cavities. In the case of U-shaped cavity crystals (Fig. 4E), the development of the hopper crystals is subsequent to the tabular form (Fig. 11A, 1–3). For V-shaped cavity crystals (Fig. 4D), the tabular morphology is not observed in the centre of the hopper cavity. Therefore, V-shaped cavity crystals can be considered as a real hopper form. Indeed, as they do not derive from tabular crystals they nucleate and grow in the stability field of the hopper habit (Fig. 11 B, 1 and 2).

The fact that these two crystalline shapes are present in the same sample can be explained if we consider that the heterogeneous nucleation of olivine crystals on platinum fragments proceeds throughout the cooling. Therefore, hopper shapes can nucleate late and directly on a platinum fragments (V-shape) or as an overgrowth on crystalline tablets (U-shape). The result is that the V-shaped crystals are generally smaller than U-shaped grains within the same charge (Fig. 11A3 and B2).

Beginning of dendritic growth: baby swallowtail morphology

Initiation of dendritic growth corresponds to the formation of overgrowths on the previously developed hopper crystals. These overgrowths have a “half hopper shape”, and are always situated inside the cavity of the hopper crystal. However, such an occurrence is not in

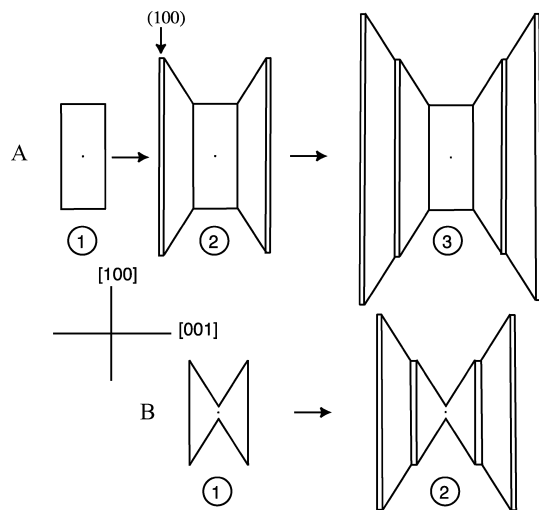


Fig. 11 Development of scenario for hopper shape. **A** Large hopper crystals show all the development steps from tabular habit (1) to hopper shape (2 and 3). The flat bottom of the hole is due to tabular growth stage. **B** If the tabular stage did not occur, only the hopper morphology exists (1 and 2) and the hole has a pointed shape

agreement with the so-called Berg effect (1938). The latter predicts that the growth of dendrites is highly favoured in regions that present the higher supersaturation rate in chemical species. It is thus expected that dendrites will preferentially develop on the corners of hopper crystals. The “Berg effect” has been confirmed experimentally in the case of growth from low-temperature solution (Kern 1953; Follenius 1959), and also from silicate melt (high-temperature solution growth), notably for olivine (Kirkpatrick et al. 1981).

This apparent contradiction between our observations (Fig. 5) and the expected location for dendrites on the basis of the Berg theory can be resolved if we consider that the parent hopper crystal grows faster than the overgrowths. Indeed, if the dendritic overgrowths nucleate as expected in the corner of hopper crystals, and if the hopper crystal grows faster than these overgrowths, the latter are then trapped inside the cavity of the parent hopper crystal. On the other hand, if overgrowths grow faster than parent hopper crystal, the growth of the hopper crystal is stopped. Thus, baby swallowtail crystals illustrate a competition process in the growth of both dendrites and parent hopper crystals.

Figure 12 is a schematic illustration of such competition processes. The overgrowths (future dendrites) start to grow on a very small (100) face situated just near the corner of the cavity (Fig. 12A). When the hopper crystal grows faster than the overgrowths, the growth of dendrite is impeded, as these crystals are not situated in an optimal condition of growth (supersaturation) due to the Berg effect. Therefore, a new generation of overgrowths situated in the external part of the hopper appear (Fig. 12B). If the overgrowths grow faster than the parent hopper crystal, the growth of the hopper crystal stops in this region (Fig. 12B–D). This situation is

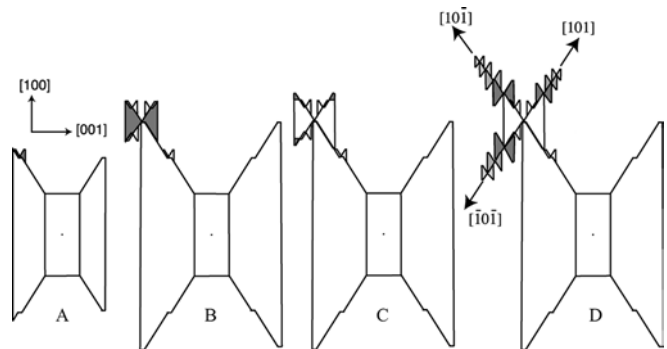


Fig. 12 Development of scenario for the dendritic morphology which could result from a competition between hopper crystal and overgrowths. **A** The overgrowth always commences on the external corner of the hopper crystal. When hopper crystal grows faster than overgrowth, this later stops its growth and a new generation of overgrowth appears (**B**). **B** The new generation of overgrowth grows faster than the hopper crystal and the growth of the hopper crystal stops in the zone near overgrowths. The new generation develops overgrowths as well. **C** As previously for overgrowth hopper crystal, a competition develops between the old and the new overgrowths. **D** Dendritic morphology results from the accumulation of overgrowths with a hopper shape

observed in Fig. 5G, in which different growth steps have been reconstructed (Fig. 5H):

- the hourglass shape first develops (labelled 1 in Fig. 5H),
- a large overgrowth forms (labelled 2), followed by a second generation of overgrowths (labelled 3) which appears on the first one.

The second generation of crystals prevents the hourglass shape growing in this area, whereas the crystalline area of hourglass shape which is not in competition with overgrowths can grow (labelled 4). This means that overgrowths and hopper crystal have different growth rates (and hence growth mechanisms) for a given degree of undercooling. At the beginning of the crystallisation process, the growth rate of hopper crystal is higher than that of the overgrowth, while this order is reversed later on during cooling.

The resulting dendrite morphology

The final morphology of dendrite (swallowtail crystal) corresponds to extended (010) lamellae that are very thin. Dendrites are composed of fibres and the latter are slightly arching in the (010) plane. This macroscopic geometry is clear in an SEM image (Fig. 7), as well as in optical microscopy observations. Nevertheless, dendrites extinguish homogeneously. This arching phenomenon can be explained with Fig. 12. To a first approximation, a [101] fibre (see Fig. 12D) is formed by the juxtaposition of several hopper crystals, whose average size decreases from the centre (parent hopper crystal) to the periphery of the dendrite. These hopper crystals, lined up to form a fibre, are not in the same plane (Fig. 13). Each new hopper crystal takes place inside a previous one and then, a vicinal (010) face is formed. This interpretation accounts for the arched shape of the crystals.

When the parent hopper crystal is large, the cavity of the crystal is large as well. Then, several sets of hopper crystals can nucleate simultaneously and grow at the same time inside the same cavity. This situation leads to the formation of several (010) dendrite lamellae which are parallel and which exhibit the same orientation. This explains why all the parallel rods, observed in a thin section by optical microscopy, have a common extinction. Therefore, sets of parallel rods (cross sections of the dendrite lamellae) should be more frequently

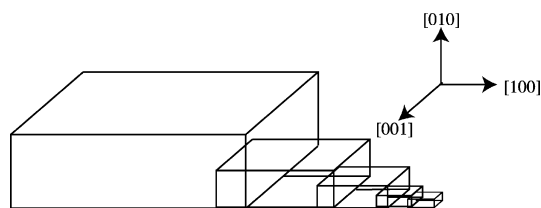


Fig. 13 Schematic illustration showing the arching shape of a dendritic fibre

observed in rocks that are cooled quite slowly, as slow cooling rate is the main condition to enhance the formation of large cavities in the [010] direction of the hopper crystals.

Experimental tests of the dendrite morphology model

The model presented above implies that dendrites always correspond to the repetition in three dimensions of the same unit, a hopper shape. This model is coherent with the fact that dendritic olivine presents fractal dimension (Fowler et al. 1989) and is thus composed of connected fractal objects. The size of hopper crystal progressively decreases from the centre of the crystal to the periphery of the dendrite, as the last generation of hopper crystals has not the time to grow (Fig. 14A, step b). Thus, in a specific series of experiments, we reheated samples in order to enhance crystal growth (Fig. 14A, step c) before quenching. This annealing treatment has been carried out in order to increase the size of the crystals at the tips of the dendrites. This experiment was successful and the result is presented in Fig. 14C. Those crystals clearly display a hopper shape. In an another set

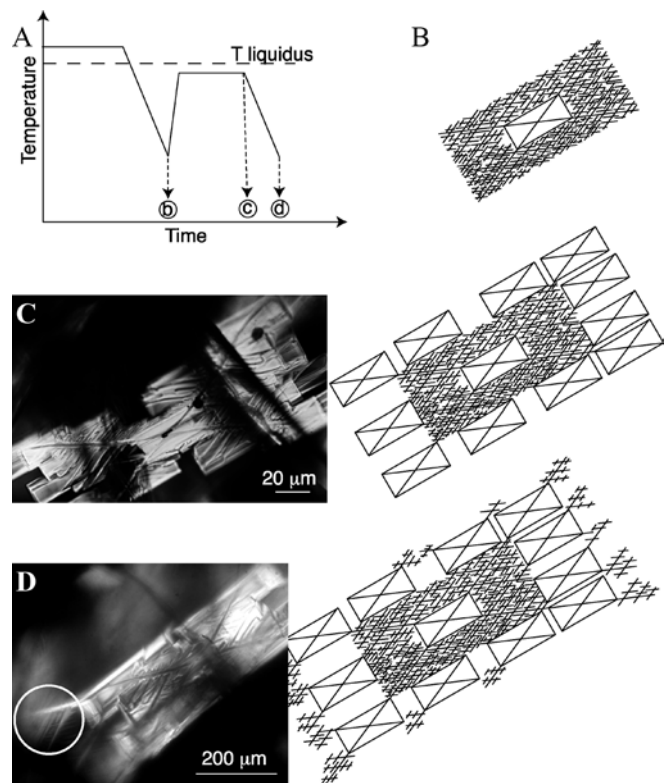


Fig. 14 Experimental tests of the model. **A** Schematic illustration of the experimental conditions. **B** Typical swallowtail crystal obtained in constant cooling rate experiment (e.g. Fig. 6 A). **C** Swallowtail crystal is re-heated below the liquidus temperature to increase the size of the last unit of dendritic fibres. Dendritic tips display a hopper shape. **D** Swallowtail crystals re-heated in C then cooled at constant rate in order to develop dendrites (circled area) in the hopper shapes at the tips of the first dendrites

of experiments, the same samples were submitted to an additional treatment with fast cooling rate (Fig. 14A, step d). Figure 14D shows that under those conditions, the newly former hopper crystals evolve toward dendritic shape as already observed for all parent hopper crystals that form swallowtail shape.

Conclusion

The numerous experiments performed to grow olivine crystals at various cooling rates and degrees of undercooling allow identification of two types of growth mechanisms, a steady-state regime under which polyhedral crystals are developed and a rapid growth regime which eventually results in the formation of dendrites. The rapid growth state is shown to be mainly influenced by the degree of undercooling with minor influence of the cooling rate. In response to the increased undercooling parameter, the morphology of rapid growth evolves from tablet crystal to dendrites in the following sequence: tablet⇒hopper crystal (hourglass shape)⇒incipient dendrite (baby swallowtail crystal)⇒dendrite (swallowtail morphology).

During the dendrite formation, these different steps are observed. However, this is not systematic and some may be lacking, depending on the timing of nucleation of tablet and hopper with regard to the beginning of the formation of incipient dendrites (baby swallowtail crystals). This study shows that the formation of dendrites relies on overgrowth of small hopper crystals, in agreement with the fractal model proposed for olivine dendrites (Fowler et al. 1989). These hopper crystals are aligned in the [101] and [-101] directions, forming fibres. Several generations of hopper crystals are involved, giving rise to several generations of fibres. These different generations of fibres are shown to be in competition. Complex heating treatments performed during the formation of dendrites clearly demonstrate that modulation of the degree of undercooling during the growth of dendrites modifies the size of the peripheral hopper crystal which forms the fibres.

These variations of hopper or dendrite olivine shapes with regard to the normal morphologies (none annealed hopper or dendrite crystals) obtained in dynamic crystallization experiments could allow the petrologist to determine the complex thermal history of some volcanic rocks such as pillow-lavas (Faure et al., in preparation).

However, it is important to keep in mind that even if olivine morphologies in these experiments are similar to morphologies observed in rocks, absolute cooling rate estimates for the rocks is strongly dependant of presence (or absence) of nuclei at the initiation of cooling (Schiffman and Lofgren 1982). Therefore, the pre-eruptive history of the magma must be known before.

Acknowledgements We have benefited from discussions with many colleagues, including A. Baronnet, B. Devouard, T. Hammouda,

D. Laporte, P. Boivin and A. Provost. The authors wish to thank G. Lofgren and C.H. Donaldson for their useful review.

References

- Arndt J, Engelhardt WV (1987) Formation of Apollo 17 orange and black glass beads. *Proc 15th Lunar Planet Sci Conf* 92, pp 372–376
- Arndt J, Engelhardt WV, Gonzalez-Cabeza I, Meier B (1984) Formation of Apollo 15 green glass beads. *Proc 15th Lunar Planet Sci. Conf* 89, pp 225–232
- Arndt NT (1986) Differentiation of komatiite flows. *J Petrol* 27:279–301
- Barnes SJ (1998) Chromite in komatiites, 1. Magmatic controls on crystallization and composition. *J Petrol* 39:1689–1720
- Berg WF (1938) Crystal growth from solutions. *Proc R Soc* 164:79–95
- Berkebile CA, Dowty E (1982) Nucleation in laboratory charges of basaltic composition. *Am Mineral* 67:886–899
- Bryan WB (1972) Morphology of quench crystals in submarine basalts. *J Geophys Res* 77: 5812–5819
- Chernov AA, Nishinaga T (1987) Growth shapes and their stability at anisotropic interface kinetics: theoretical aspects for the solution growth. In: Sunagawa I (ed) *Morphology of crystals*. Terra Scientific Publishing Company, Tokyo, pp 207–268
- Coish RA, Taylor LA (1979) The effects of cooling rate texture and pyroxene chemistry. In: *DSDP LEG 34 basalt: a microprobe study*. *Earth Planet Sci Lett* 42:389–398
- Deer WA, Howie RA, Zussman J (1962) *Orthosilicates*, Longman Group Ltd, London
- Donaldson CH (1976) An experimental investigation of olivine morphology. *Contrib Mineral Petrol* 57:187–213
- Donaldson CH (1977) Laboratory duplication of comb layering in the Rhum pluton. *Mineral Mag* 41:323–336
- Donaldson CH (1982) Spinifex-textured komatiites: a review of textures, compositions and layering. In Arndt NT, Nisbet EG (eds) *Komatiites*. Allen and Unwin, London, pp 213–244
- Donaldson CH, Williams RJ, Lofgren G (1975a) A sample holding technique for study of crystal growth in silicate melts. *Am Mineral* 60:324–326
- Donaldson CH, Williams TM, Lofgren GE (1975b) Experimental modeling of the cooling history of Apollo 12 olivine basalts. *Proc 6th Lunar Sci Conf*, pp 843–870
- Drever HI, Johnston R (1957) Crystal growth of forsteritic olivine in magmas and melts. *Trans R Soc Edinb* 63:289–315
- Faure F (2001) Les textures de croissance rapide dans les roches magmatiques basiques et ultrabasiques: étude expérimentale et nanoscopique. PhD Thesis, Univ Clermont-Ferrand
- Faure F, Troliard G (1999) Dynamic crystallization of forsterite: experimental and TEM investigations. *EUG 10, Strasbourg, J Conf Abs* 4, p 676
- Faure F, Troliard G, Montel JM, Nicollet C (2001a) Nanopetrographic investigation of a mafic xenolith (maar de Beaunit, Massif Central France). *Eur J Mineral* 13:27–40
- Faure F, Troliard G, Montel JM, Soulestin B (2001b) Morphology of forsterite dendrites. *EUG 11, Strasbourg, J Conf Abs* 6, p 539
- Follenius M (1959) Application d'une méthode interférométrique en lumière blanche polarisée à l'étude de la croissance cristalline. *Bull Soc Fr Minér Crist* 82:343–360
- Fowler AD, Stanley HE, Daccord G (1989) Disequilibrium silicate mineral textures: fractal and non-fractal features. *Nature* 341:134–138
- Hewins RH, Klein LC, Fasano BV (1981) Conditions of formation of pyroxene excentroradial chondrules. *Proc 12th Lunar Planet Sci*, pp 1123–1133
- Jambon A, Lussiez P, Clocchiatti R, Weisz J, Hernandez J (1992) Olivine growth rates in a tholeiitic basalt: An experimental study of melt inclusions in plagioclase. *Chem Geol* 96:277–287

- Keith HD, Padden FJ (1963) A phenomenological theory of spherulitic crystallization. *J Appl Phys* 34:2409–2421
- Kern R (1953) Etude du faciès de quelques cristaux ioniques a structure simple. *Bull Soc Fr Miner Crist* 76:325–391
- Kirkpatrick RJ (1978) Processes of crystallization in pillow basalts, hole 396B, DSDP LEG 46. In: Dmitriev L, Heirtzler J et al. (eds) Initial reports of the Deep Sea Drilling Project 46. US Govt Printing Office, Washington, pp 271–282
- Kirkpatrick RJ, Hodges FN (1978) Crystallization of the core 15 basalt cooling unit, hole 396B, DSDP LEG 46. In: Dmitriev L, Heirtzler J et al. (eds) Initial reports of the Deep Sea Drilling Project 46. US Govt Printing Office, Washington, pp 259–269
- Kirkpatrick RJ, Kuo LC, Melchior J (1981) Crystal growth in incongruently-melting compositions: programmed cooling experiments with diopside. *Am Mineral* 66:223–241
- Kirkpatrick RJ, Reck BH, Pelly IZ, Kuo LC (1983) Programmed cooling experiments in the system MgO-SiO₂: kinetics of a peritectic reaction. *Am Mineral* 68:1095–1101
- Lofgren G (1971) Spherulitic textures in glassy and crystalline rocks. *J Geophys Res* 76: 5635–5648
- Lofgren G (1975) Dynamic crystallization experiments on mare basalts. In: Origins of mare basalts and their implications for lunar evolution. Lunar Science Institute, Houston, pp 99–103
- Lofgren G (1980) Experimental studies on the dynamic crystallization of silicate melts. In: Hargraves RB (ed) Physics of magmatic processes. Princeton University Press, Princeton, pp 487–551
- Lofgren GE (1983) Effect of heterogeneous nucleation on basaltic textures: A dynamic crystallization study. *J Petrol* 24:229–255
- Lofgren G (1989) Dynamic crystallization of chondrule melts of porphyritic olivine composition: textures experimental and natural. *Geochim Cosmochim Acta* 53:461–470
- Lofgren G (1996) A dynamic crystallization model for chondrule melts. In: Hewins RH et al. (ed) Chondrules and the protoplanetary disk. Cambridge University Press, Cambridge, pp 187–196
- Lofgren G, Russell WJ (1986) Dynamic crystallization of chondrule melts of porphyritic and radial pyroxene composition. *Geochim Cosmochim Acta* 50:1715–1726
- Lofgren GE, Donaldson CH (1975) Curved branching crystals and differentiation in comb-layered rocks. *Contrib Mineral Petrol* 49:309–319
- Natland JH (1979) Crystal morphologies in basalts from DSDP site 395 23°N, 46°W, mid-Atlantic ridge. Initial reports of the Deep Sea Drilling Project 46, pp 423–445
- Ohnenstetter D, Brown WL (1992) Overgrowth textures, disequilibrium zoning, and cooling history of a glassy four-pyroxene boninite dyke from New Caledonia. *J Petrol* 33:231–271
- Presnall DC, Dixon SA, Dixon JR, O'Donnell TH, Brenner NL, Schrock RL, Dycus DW (1978) Liquidus phase relations on the join diopside-forsterite-anorthite from 1 atm to 20 kbar: Their bearing on the generation and crystallization of basaltic magma. *Contrib Mineral Petrol* 66:203–230
- Renner R, Nisbet EG, Cheadle MJ, Arndt NT, Bickle MJ, Cameron WE (1994) Komatiite flows from the Reliance formation, Belingwe Belt, Zimbabwe: 1. Petrography and mineralogy. *J Petrol* 35:361–400
- Schiffman P, Lofgren GE (1982) Dynamic crystallization studies on the Grande Ronde pillow basalts, central Washington. *J Geol* 90:49–78
- Smit J, Alvarez W, Montanari A, Burne NS, Kempen TMV, Klaver GT, Lustenhouwer WJ (1992) “Tektites” and microkrystites at the Cretaceous Tertiary boundary: Two strewn fields, one crater? *Proc Lunar Planet Sci* 22:87–100
- Sunagawa I (1981) Characteristics of crystal growth in nature as seen from the morphology of mineral crystals. *Bull Mineral* 104:81–87
- Sunagawa I (1987) Morphology of minerals. In: Sunagawa I (eds) Morphology of crystals. Terra Scientific Publishing Company, Tokyo, pp 509–587
- Techmer KS, Echer C, Wenk HR (1996) SEM and TEM/AEM studies of crystallization processes in some natural glasses (pseudotachylites of the Ivrea-Verbano zone, northern Italy and quenched volcanic rocks from Mono Lake, California). *Chem Erde* 56:373–378
- Walker D, Kirkpatrick RJ, Longhi J, Hays JF (1976) Crystallization history of lunar picrite basalt sample 12002: phase equilibria and cooling-rate studies. *Geol Soc Am Bull* 87:646–656